NJC

PAPER

View Article Online
View Journal | View Issue

Cite this: *New J. Chem.*, 2024, 48, 9627

Circularly polarized luminescence activity in the near infrared spectral region of a water-soluble ytterbium(III) complex containing a conjugated chromophoric ligand†

Silvia Mizzoni, [ab] Annika Sickinger, [b] Silvia Ruggieri, [a] François Riobé, [b] Laure Guy, [b] Olivier Maury, *[b] Bruno Baguenard, [c] Amina Bensalah-Ledoux, [c] Yannick Guyot, [c] Stéphan Guy, [c] Martina Sanadar, [d] Andrea Melchior *[d] and Fabio Piccinelli *[a]

Received 1st February 2024,
Accepted 3rd April 2024

DOI: 10.1039/d4nj00550c

rsc.li/njc

Two cationic enantiomeric complexes [(*R*,*R*)-[Yb**L**]Cl and (*S*,*S*)-[Yb**L**]Cl with **L** = *N*,*N*′-bis(2-pyridylmethyl)-1,2-(*R*,*R* or *S*,*S*)-cyclohexanediamine functionalized at sp^3 N with picolinate *antennae*] have been synthesized and spectroscopically characterized in polar protic solvents, such as water and methanol. The Yb(III) luminescence at about 980 nm is efficiently sensitized upon excitation of the picolinate antenna in the UV spectral region around 330 nm. The complexes exhibit good CPL activity for the $^2F_{5/2} \rightarrow {}^2F_{7/2}$ magnetic dipole (MD) allowed transition (g_{lum} values of |0.02| and |0.04| at 984 nm and 1021 nm, respectively) and high solubility in aqueous solution. The Yb**L** species is largely predominant at physiological pH (7.4), given its high thermodynamic stability ($\log \beta_{Yb}$**L** = 20.98). As elucidated by DFT calculations, among the possible isomeric species the one characterized by the *cis*-O, O–N, N geometry was found to be dominant. Furthermore, one solvent molecule is bound to Ln(III) in water, giving rise to 9-fold coordination at the metal ion. The enantiomeric (*R*,*R*)-[Yb**L**]Cl and (*S*,*S*)-[Yb**L**]Cl complexes can be considered promising candidates as NIR-to-NIR chiroptical bioprobes also for *in vivo* experiments.

Introduction

Materials chemistry and physics are increasingly pervaded by the possible technological application of circularly polarized luminescence (CPL).[1,2] In particular, during the last few years the scientific community working in the field of chiral lanthanide(III)-based complexes has shown interest in the investigation of materials emitting CPL in the near-infrared (NIR) spectral region.[3–13]

The specificity, selectivity and sensitivity which are typical of the chiroptical counterpart of emission spectroscopy (*i.e.*, CPL) stemming from lanthanide(III) ions have proven to be very important in the context of biological applications, such as microscopy and bioassays.[14–17] Only recently Stachelek *et al.* were able to determine, thanks to CPL, the enantioselective localization of the two enantiomeric Eu(III) complexes in two different cell environments (lysosomes and mitochondria).[18] This contribution paves the way for the potential and unprecedented use of CPL in *in vivo* bioimaging experiments. So far, the use of chiroptical probes working in the near-infrared spectral region is still quite limited and the design of new NIR-to-NIR chiroptical probes would have a significant impact on their biological applications. Recently, some of us demonstrated that the Yb(III) luminescence can be efficiently sensitized upon excitation of a conjugated ligand system in different spectral regions: from UV to Vis.[19,20] In order to efficiently sensitize the Ln(III) luminescence at NIR wavelengths, one possible strategy is the design of ligands including a two-photon absorbing chromophoric *antenna* capable of transferring the excitation energy to the Ln(III) ion. Two-photon (2P) excitation is a non-linear optical phenomenon which takes place when an excited state of a chromophore can be populated by the concomitant absorption of two photons, whose wavelength is twice that of

[a] *Luminescent Materials Laboratory, DB, Università di Verona, and INSTM, UdR Verona, Strada Le Grazie 15, 37134 Verona, Italy. E-mail: fabio.piccinelli@univr.it*
[b] *Univ Lyon, ENS de Lyon, CNRS UMR 5182, Laboratoire de Chimie, Lyon F-69342, France. E-mail: olivier.maury@ens-lyon.fr*
[c] *Univ. Lyon, Institut Lumière Matière, UMR 5306 CNRS–Université Claude Bernard, 10 rue Ada Byron, Lyon 1, F-69622 Villeurbanne Cedex, France*
[d] *Dipartimento Politecnico di Ingegneria e Architettura, Laboratorio di Tecnologie Chimiche, Università di Udine, via Cotonificio 108, 33100 Udine, Italy. E-mail: andrea.melchior@uniud.it*

† Electronic supplementary information (ESI) available. See DOI: https://doi.org/10.1039/d4nj00550c

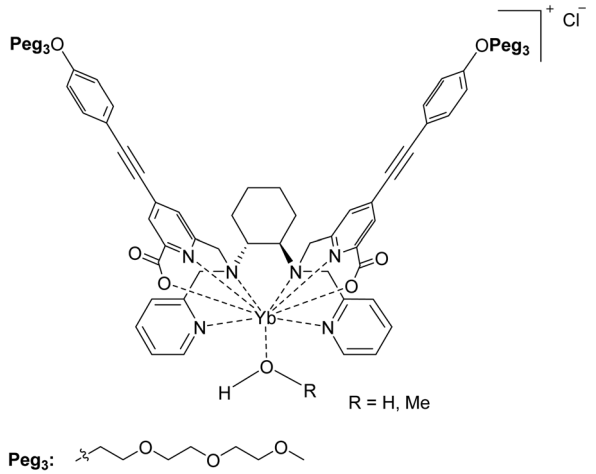

Fig. 1 (*S*,*S*)-[Yb**L**]Cl complex discussed in this contribution. Also the (*R*,*R*) enantiomer is considered in this work.

the single photon excitation. This technique has been already conveniently employed in Ln(III)-based coordination compounds with potential biological applications.[21–23] If the two-photon absorption phenomenon allows shifting of the excitation wavelength from UV (1P excitation) to NIR (2P excitation) the proper choice of the Ln(III) ions enables to produce NIR emission. Indeed, as we previously demonstrated, the luminescence of an Eu(III) complex (at 620 nm) can be sensitized upon NIR excitation (around 720 nm).[24] In this context, the analogous Yb(III) complex bears high potential for in cellulo experiments as a NIR-to-NIR optical probe[23] that is active in the short wavelength range of the so-called "biological window" (650–1450 nm).

As a logical extension of a recent work in which the Eu(III) and Sm(III) chiral complexes of ligand **L** [which is *N*,*N*′-bis(2-pyridylmethyl)-1,2-(*R*,*R* or *S*,*S*)-cyclohexanediamine functionalized at sp^3 N with the picolinate antennae; Fig. 1] have been in-depth investigated,[24] we synthesized and spectroscopically characterized in this contribution both the enantiomers of the chiral Yb(III)-based counterpart [namely (*S*,*S*)-[Yb**L**]Cl and (*R*,*R*)-[Yb**L**]Cl complexes depicted in Fig. 2]. The presence of conjugated picolinate *antennae* ensures 2P absorption features and thanks to a ligand-to-metal energy transfer process (*antenna effect*) the metal-centered luminescence can be triggered, like in the case of Eu(III) and Sm(III) complexes. We also demonstrated that the octadentate ligand system enables the emission of circularly polarized (CP) light by the coordinated Ln(III). All these aspects make this pair of complex enantiomers ideal candidates for emerging chiroptical applications in the field of *in vivo* bioimaging.

Experimental section

General

All reactions of air- and/or water-sensitive compounds were carried out under an inert gas atmosphere using standard Schlenk techniques. Solvents were purchased from Fisher Scientific, VWR Chemicals or Carlo Erba Reagents and used without further purification. All the solvents used for the synthesis were stored over 3 Å molecular sieves. Starting materials were purchased from Sigma-Aldrich, TCI, Alfa Aesar or Acros Organics. Column chromatography was performed using silica gel (40–63 μm) from VWR Chemicals. IR Spectra were recorded on a Spectrum 65, 100 and 400 series FT-IR spectrometer. Typical 32 scans were accumulated for each spectrum (resolution of 4 cm^{-1}). High resolution mass spectrometry measurements (HR-MS) were performed at the Centre Commun de Spectrometrie de Masse (Villeurbanne, France) with a MicroOTOFQ II (Bruker) using electrospray ionization (ESI). Both the enantiomers of **1** and **L** (Fig. 2) have been synthesized, respectively, as reported in the literature.[24] $YbCl_3{\cdot}6H_2O$ (Aldrich, 98%) has been stored under vacuum for several days at 80 °C and then transferred into a glove box.

Synthesis of (*S*,*S*)-[YbL**]Cl and (*R*,*R*)-[Yb**L**]Cl.** The synthesis of the enantiomeric complexes (Fig. 2) was performed as follows: a

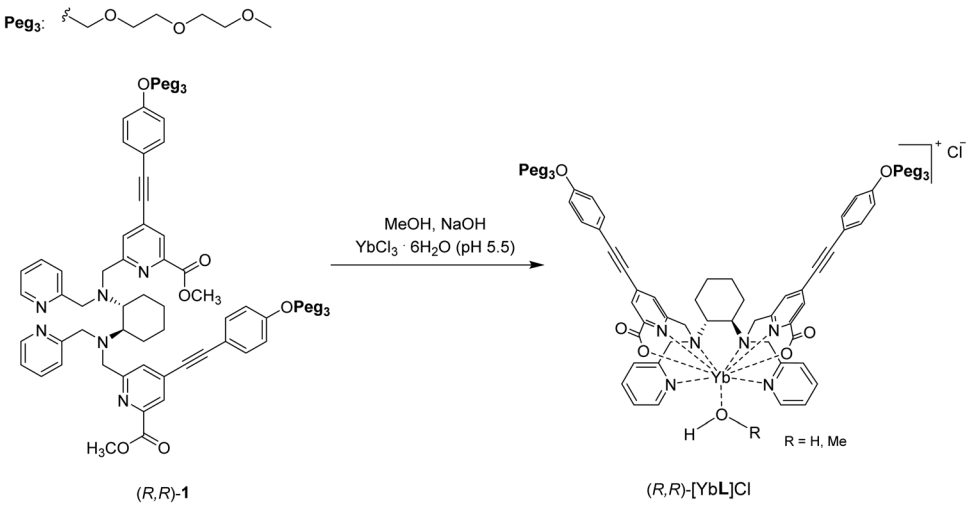

Fig. 2 Synthetic pathway for the synthesis of the (*S*,*S*) or (*R*,*R*)-[Yb**L**]Cl complexes. For the sake of simplicity, only the (*R*,*R*) enantiomer is reported.

solution of the proligand **1** (*R*,*R*) or (*S*,*S*) (0.018 mmol, 1 equiv.; see Fig. S1 for additional characterization data of **1**, ESI†) in MeOH (11 mL) and a 1 M solution of sodium hydroxide (0.16 mmol, 9 equiv.) in water (1 M) were mixed together and stirred overnight. Then, the solution was acidified until pH = 5.5 using HCl (0.1 M) and the Ln(III) chloride salt ($YbCl_3{\cdot}6H_2O$, 0.023 mmol, 1.3 equiv.) was added to the solution and left stirring overnight. Then, the reaction mixture was concentrated, and the residue was dissolved in dichloromethane and washed with water to remove salts in excess. Na_2SO_4 was added to the organic layer, and after removal of the solvent under reduced pressure, the desired complex was obtained as a pale-yellow solid. (*S*,*S*)-[Yb**L**]Cl: yield 94%; (*R*,*R*)-[Yb**L**]Cl: yield 92%.

ESI-HR-MS (positive, CH_3CN; *m*/*z*) calcd for $[C_{62}H_{68}N_6O_{12}Yb]^+$: 1262.4278, found: 1262.4268 (*S*,*S*)-[Y**L**]Cl, 1262.4275 (*R*,*R*)-[Yb**L**]Cl, $[M]^+$. See Fig. S1 (ESI†).

FT-IR (cm^{-1}, ATR): C=O: 1634; C≡C: 2206 (Fig. S2, ESI†).

Spectrophotometric titrations

Stock solutions of NaOH and HCl were prepared using Fixanal 0.1 M (Fluka Analytical) standard solution and ultrapure water (>18 MΩ cm) from a MilliQ system (ELGA Purelab UHQ). The ionic strength of all solutions was adjusted to 0.1 M with NaCl (Riedel-de Haën). Stock solutions of Yb(III) (14.6 mM) were prepared by dissolving the chloride hexahydrate salts (Sigma-Aldrich) and standardized by titration with **EDTA** and xylenol orange as the indicator in acetate buffer.[25] Stock solutions of Zn(II) (15.0 mM) and Ca(II) (17.5 mM) were prepared by dissolving the chloride hexahydrate salts (SigmaAldrich) and standardized by titration with **EDTA** and eriochrome black T as the indicator in buffer pH 10.[25] Complex formation constants were determined by combined potentiometric/UV-Vis titrations in the range pH = 1.96–11.47.[26,27] Electromotive force (emf) data were collected by using a computer-controlled potentiometer (Amel Instruments, 338 pH Meter) connected to a combined glass electrode (Metrohm Unitrode 6.0259.100). The electrode was calibrated before each lecture by acid–base titration with standard HCl and NaOH solutions. The content of carbonate in solution, as well as free acid concentrations in stock metal ion solutions, was determined using Gran's method.[28] Absorption spectra were collected using a Varian Cary 50 spectrop hotometer equipped with an optical fiber probe (1 cm optical path length) which was inserted into the titration cell which contained a solution with the ligand (total concentration = 0.016 mM) and an equimolar quantity of Yb(III)/Zn(II)/Ca(II). In all cases, the titration cells were maintained at a constant temperature (25 °C) with a circulatory bath and under Ar radial flux to avoid carbonate contamination. Absorbance data at multiple (>40) wavelengths in the 250–380 nm range were analyzed using the HypSpec program[29] to obtain the complex formation constants using the previously determined ligand pK_a (pK_a: HL = 9.65, H_2L = 8.88, H_3L = 3.60, H_4L = 2.20).[24]

DFT calculations

All molecular structures of the complexes were obtained by means of DFT calculations run in Gaussian 16 (rev. A.03).[30] The ωB97X–D functional[31] was used with the 6–31+G(d) basis set for all ligand atoms and MWB59 pseudopotential and valence electron basis set for Yb.[32] To reduce the computational cost of the geometry searches, the PEGylated chain of L has been replaced by a methyl ether group (–OCH_3). Geometry optimizations were carried including solvent (water) by means of the polarizable continuum model (PCM).[33]

Photophysical measurements

Absorption spectra were recorded using a JASCO V-650 spectrophotometer in dilute solution (*ca.* 10^{-5} or 10^{-6} M), using spectrophotometric grade solvents. Emission spectra were measured using a Horiba–Jobin–Yvon Fluorolog-3 fluorimeter. The steady-state luminescence was excited by unpolarized light from a 450 W xenon continuous wave (CW) lamp and detected at an angle of 90° for measurements of dilute solutions (10 mm quartz cuvette) by using a Hamamatsu R928 photomultiplier tube. Spectra were corrected for both excitation source light–intensity variation and emission spectral responses. For luminescence lifetimes, the sample in an EPR quartz tube was excited using a pulsed Nd:YAG laser (SpectraPhysics), operating at 10 Hz. Light emitted at right angles to the excitation beam was focused onto the slits of a monochromator (PTI120), which was used to select the appropriate wavelength. The growth and decay of luminescence at selected wavelengths were detected using a Ge photodiode (Edinburgh Instruments, EI-P) and recorded using a digital oscilloscope (Tektronix TDS320) before being transferred for analysis. Luminescence lifetimes were obtained by iterative reconvolution of the detector response (obtained by using a scatterer) with exponential components for growth and decay of the metal-centered luminescence.

Luminescence decay curves were fitted using the mono-exponential equation:

$$I(t) = I_0 \times e^{-\frac{t}{\tau}}$$

Chiroptical measurements

Measurements of circular dichroism in the UV/Vis and NIR regions were performed on a JASCO J-710 spectropolarimeter on complex solutions with concentrations around 10^{-5} (UV/Vis) and 1 M (NIR). CPL spectra were recorded with a bandwidth of 3 nm, on a homemade apparatus at the Institute of Light and Matter, Villeurbanne.[34] Solutions (10^{-4} M) in a quartz cuvette are excited by UV light from a diode (365 nm). The fluorescence is collected with a lens and separated by means of an achromatic $\lambda/4$ waveplate (451) and a polarizing beam splitter. With this arrangement, the light is split into two components of either left- or right circularly polarized light. Each arm is further imaged on one side of a fiber bundle. The other extremity of the bundle is focused on the entrance slit of a spectrophotometer. The spectrally separated light is imaged on a CCD camera. The ''upper/lower'' part of the camera records the left- or right-handed circularly polarized spectra. Because of the brightness of the molecules as well as their high g_{lum}, this

set-up allows fast recording of the CPL spectra in less than ten seconds.

Results and discussion

Synthesis of ytterbium complexes

Both complexes have been obtained in high chemical yield [94% and 92% for (*S*,*S*)-[Yb**L**]Cl and (*R*,*R*)-[Yb**L**]Cl, respectively] following the synthetic path depicted in Fig. 2. The reaction was completed after 12 hours, when the signal of the ester C=O stretching at about 1725 cm^{-1} in the FT-IR absorption spectrum disappeared (Fig. S2, ESI†). Furthermore, the presence of the peak related to the $[YbL]^+$ cation in the ESI-MS spectrum (Fig. S1, ESI†) confirmed the successful complexation reaction.

Complex formation equilibria and structure

The complexation constants for ligand **L** are reported in Table 1, along with those relative to other ligands previously studied by some of us[17] or others[35–37] (Fig. 3) for comparison.

The spectrophotometric data relative to the complex formation (Fig. 3a) were best fitted by a speciation model including the formation of four Yb species (Yb**L**, Yb**L**H, Yb**L**H_2 and Yb**L**(OH), Table 1) whose calculated molar absorbances are reported in Fig. S3 (ESI†). The speciation diagram of the Yb(III) complexes is shown in Fig. 4b, along with the molar absorbance at 332 nm (ε_{332}) as a function of pH. A marked decrease in absorbances at 313 and 332 nm between pH 2 and 4 is present in correspondence with the Yb**L**H_2 and Yb**L**H (Fig. 4b) species. At pH > 4, the Yb**L** complex starts to form, coinciding with an overall rise in ε_{332}, and continues until the pH reaches 10. Subsequently, a decrease in ε_{332} and ε_{313} is observed as the Yb**L**(OH) species begins to form.

The formation constant obtained for the Yb**L** species is comparable to that of other Ln(III) complexes with similar acyclic ligands containing picolinate chelating groups,[24,36] and compatible with the formation of an octadentate complex. The stability of the complexes with **L** experiences a slight increase from Eu(III) to Yb(III), as a consequence of the increasing charge density of the metal ion due to lanthanide contraction[38,39] as often found for Ln(III) complexes with similar open-chain ligands (Fig. 3 and Table 1).[40,41] Under physiological pH (7.4) and a **L**/Yb molar ratio of 1, the Yb**L** species is largely dominant (>98%, Fig. 4). The formation constants obtained for the complexes with other metal ions of biological importance Ca(II) and Zn(II) are significantly lower than those found for Yb(III) (Table 1 and Fig. S4, ESI†). The selectivity, similar to that previously found for the complexes formed with **octapa** and **CHXoctapa**[36] with Zn(II) and slightly higher for Ca(II) (Table 1), supports the application of Yb**L** in biological media.

The possible structures of the related Eu(III) and Sm(III) complexes in solution were previously proposed on the basis of DFT calculations.[24] In the case of Yb(III), the complexes result to be isostructural with those obtained previously for Y(III), with the water molecule retained in the coordination sphere. This result was not predictable, as the decrease of the ionic radius of the lanthanide can cause a decrease of the coordination number, as observed in complexes with macrocyclic polyaminocarboxylic

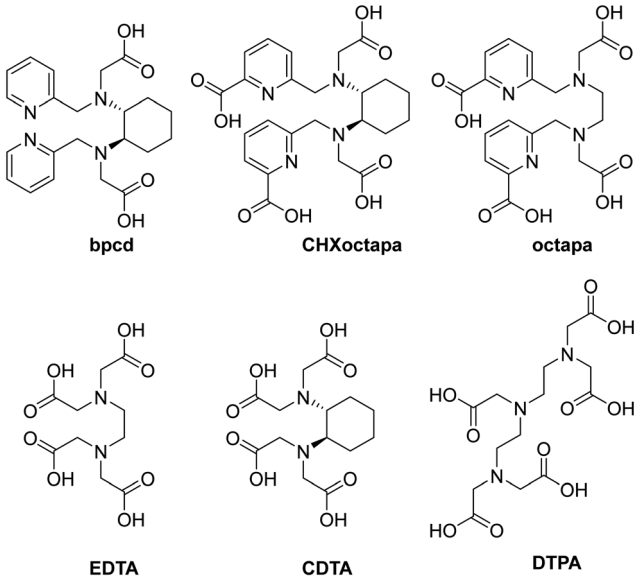

Fig. 3 Structural formulas of a series of hexa- and octadentate ligands similar to **L**.

Table 1 Complex formation constants (log β) for ligand **L** with Yb(III), Ca(II) and Zn(II) obtained at 25 °C in NaCl 0.1 M. Additional complex formation constants data with other ligands in Fig. 3 are also reported as a comparison. Charges omitted for clarity

Equilibrium	**L**	**bpcd**[17]	**CHXoctapa**[36]	**octapa**	**EDTA**[35]	**CDTA**[35]	**DTPA**[35]
L + Yb ⇋ Yb**L**	20.98 ± 0.05	—	19.65	20.10[37]	19.6	21.2	22.7
Yb**L** + H ⇋ Yb**L**H	4.29 ± 0.05	—	1.89	3.14[37]	—	—	—
Yb**L**H + H ⇋ Yb**L**H_2	3.05 ± 0.04	—	—	—	—	—	—
Yb**L**(OH) + H ⇋ Yb**L**	11.84 ± 0.05	—	12.24	10.32[37]	—	—	—
L + Eu ⇋ Eu**L**	20.13[24]	11.20	—	—	17.3	19.6	22.5
Eu**L** + H ⇋ Eu**L**H	4.69[24]	—	—	—	—	—	—
Eu**L**H + H ⇋ Eu**L**H_2	2.76[24]	—	—	—	—	—	—
L + Ca ⇋ Ca**L**	8.29 ± 0.01	—	8.42	9.55[36]	10.5	13.1	10.7
Ca**L** + H ⇋ Ca**L**H	—	—	4.83	3.92[36]	—	—	—
L + Zn ⇋ Zn**L**	18.57 ± 0.17	—	16.97	18.91[36]	16.5	19.4	18.3
Zn**L** + H ⇋ Zn**L**H	4.79 ± 0.18	—	4.04	3.91[36]	—	—	—
Zn**L**H + H ⇋ Zn**L**H_2	3.86 ± 0.19	—	3.15	3.54[36]	—	—	—
Zn**L**H_2 + H ⇋ Zn**L**H_3	2.96 ± 0.17	—	1.34	—	—	—	—
Zn**L**(OH) + H ⇋ Zn**L**	8.52 ± 0.17	—	11.63	—	—	—	—

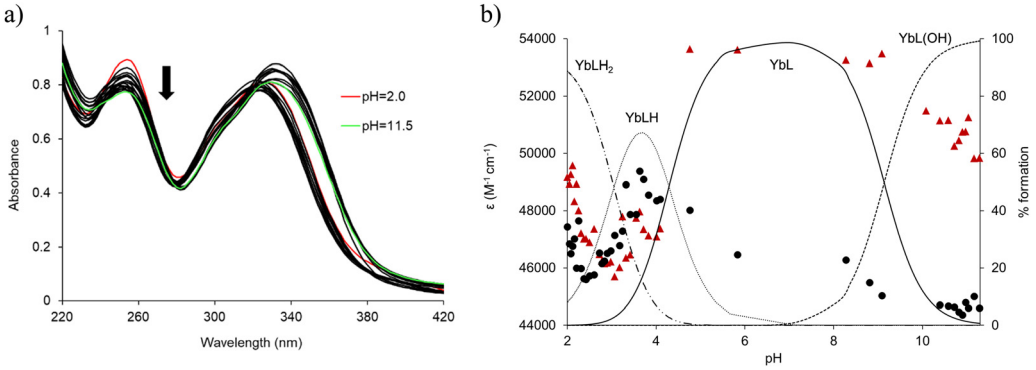

Fig. 4 (a) UV-vis absorption spectra changes during the acid–base titration of the ligand **L** (0.016 mM) in the presence of an equimolar quantity of Yb(III); (b) evolution of the molar absorbance (ε) at λ = 313 (●) and 332 (▲) nm during the titration and species distribution relative to the total metal in solution calculated on the basis of the equilibrium constants in Table 1. Charges are omitted for clarity.

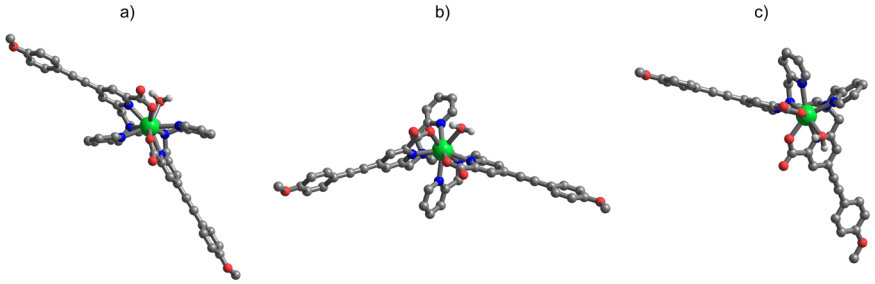

Fig. 5 Minimum energy structures of the considered (*S*,*S*) isomers of the [Yb**L**]$^+$ complex: (a) *trans*-O,O (b) *trans*-N,N, (c) *cis*-O,O–N,N. Structures are aligned along the 1,2-diaminocyclohexane moiety and hydrogen atoms are hidden for clarity. Color codes: Yb (green), O (red), N (blue) H (white), C (grey).

ligands.[42] As previously found,[24] the *trans*-O,O and *trans*-N,N isomers (Fig. 5a and b respectively) are practically equal in energy (ΔE < 0.1 kcal mol^{-1}), while the *cis*-O,O–N,N isomer (Fig. 5c) (4.2 kcal mol^{-1}) is more stable, and therefore it can be proposed as the dominant species in solution.

Photophysical properties

The absorption (λ_{max}, ε_{max}), emission [$^2F_{5/2}$ lifetime of Yb(III)] and chiroptical properties [CD (g_{abs}) and CPL (g_{lum})] of the Yb complexes have been studied in water and methanol solutions and all the relevant data are reported in Table 2.

The absorption spectra, in general independent of the nature of the lanthanide ions, are identical to the ones recorded for the Eu and Sm-based counterparts.[24] In water, they show two strong absorption peaks at 254 nm (ε around 40 000 M^{-1} cm^{-1}) and 336 nm (ε around 44 000–47 000 M^{-1} cm^{-1}) (Fig. 6).

The transition at 245 nm is related to the pyridine ring absorption[17] whilst the broad and structureless band centered at 336 nm is assigned to the ILCT transition. The typical $^2F_{5/2} \leftarrow {}^2F_{7/2}$ Yb(III) absorption band in the NIR spectral range around 980 nm is also present (Fig. 6, up, right). Due to the parity forbidden nature of the f–f lanthanide(III) transition, the molar extinction coefficient (around 5 M^{-1} cm^{-1}) is four orders of magnitude lower, compared to the transitions in the UV range discussed above. Almost identical conclusions can be drawn when the absorption spectra were collected in methanol (Fig. S5, ESI†).

While the absorption spectra in both the UV/Vis and the NIR regions are identical for the two complex enantiomers, their differential absorption of left- and right-handed CP light was demonstrated by electronic circular dichroism (ECD) measurements. In both methanol and aqueous solutions, the spectra exhibit the characteristic mirror image structure for the two enantiomers (Fig. 6, bottom and Fig. S5, ESI†). In addition to the ligand-based effect observable in the UV/Vis spectral range, the ECD was also investigated in the NIR region using concentrated solutions ($c \approx$ 1.5 M).

As for the complexes in aqueous solution, upon excitation at 333 nm (in the ILCT transition), the typical NIR emission pattern of Yb(III) is induced (Fig. 7, left).

This demonstrated the occurrence of an antenna effect involving the picolinate-based conjugated chromophore. At room temperature, the Yb(III) emission is broad and poorly resolved with a shoulder at higher energy assigned to the "hot band" originated for thermally populated m_J excited microstates (1′–0). In order to increase the resolution, low temperature (77 K) measurements were conducted in an organic glass. In this condition, the hot band disappeared and the spectra are more resolved with the clear observation of four distinct transitions (0′ → 0–4) as expected for the $^2F_{7/2}$ ground state crystal field splitting (Fig. 7, right). Despite the low temperature, a close inspection of this spectrum reveals the presence of a broader band in the 1000–1015 nm range with respect to the

Table 2 Photophysical data of the ytterbium complex in different solvents at room temperature

Complex	Solvent	λ_{max} (nm)	ε_{max} (M^{-1} cm^{-1})	τ (μs)	g_{abs}	g_{lum}
(*S*,*S*)-[Yb**L**]Cl	H_2O	333 979	44 000 4	1.0 (8.6)[a]	0.0002 (259 nm) 0.0002 (302 nm) −0.0001 (948 nm) 0.0003 (982 nm)	−0.008 (970 nm) 0.024 (984 nm) −0.034 (1021 nm)
	MeOH	336 979	51 800 9	3.4 (10.2)[b]	0.0003 (259 nm) 0.0004 (285 nm) −0.001 (942 nm) 0.003 (978 nm)	0.015 (980 nm) −0.038 (1023 nm)
(*R*,*R*)-[Yb**L**]Cl	H_2O	333 979	46 600 5	0.9 (8.5)[a]	−0.0002 (259 nm) −0.0003 (302 nm) 0.0002 (948 nm) −0.0004 (982 nm)	0.017 (970 nm) −0.017 (984 nm) 0.043 (1021 nm)
	MeOH	336 979	52 500 11	3.3 (9.5)[b]	−0.0004 (259 nm) −0.0005 (285 nm) 0.001 (942 nm) −0.003 (978 nm)	−0.013 (980 nm) 0.038 (1023 nm)

[a] = Deuterated water. [b] = Deuterated methanol.

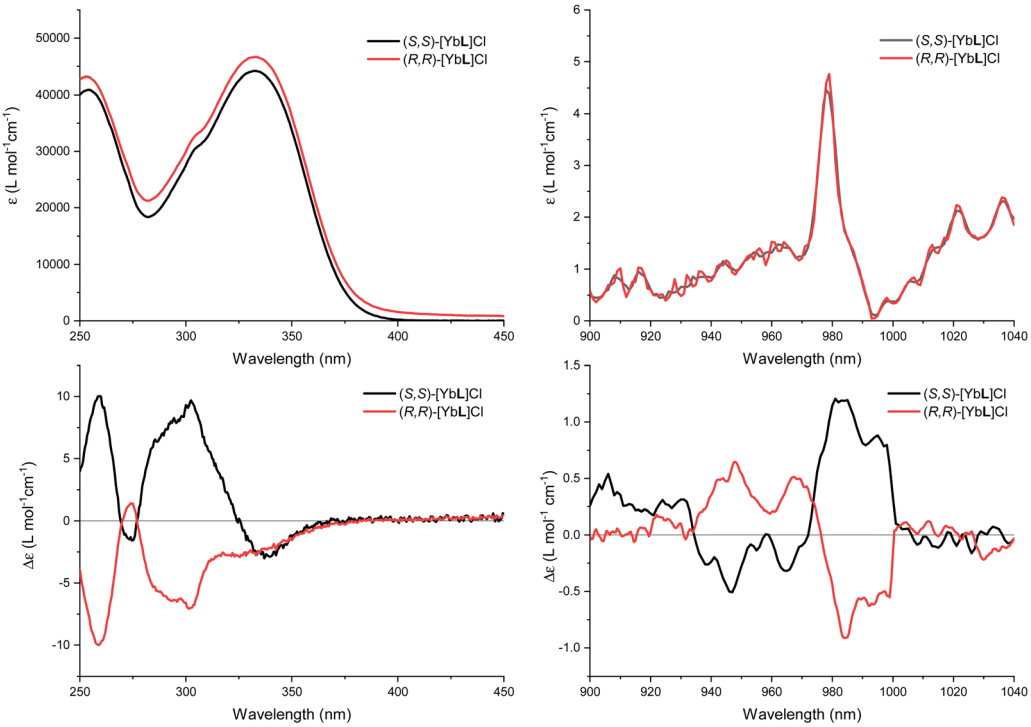

Fig. 6 Room temperature absorption spectra of both the enantiomers of [Yb**L**]Cl in the UV-Vis range (10^{-6} M aqueous solution) (up, left) and in the IR range (1.5 M aqueous solution) (up, right) and their ECD spectra in the UV-Vis range (10^{-5} M aqueous solution) (bottom, left) and in the IR range (1.5 M aqueous solution) (bottom, right).

0′–1 and 0′–3 transitions. This can be due to the presence of 1′ → (1/2/3) transitions that, even though very weak, can contribute to broaden the peak attributed to the 0′–2 peak. Alternatively, another possible explanation is that the vibronic coupling, quite important in Yb(III) electronic emission and absorption spectra, can affect the 0′–2 transition more in these complexes.

The photophysical properties of the *S*,*S*-[Gd**L**]Cl complex have been recently published in order to determine the energy diagram of the coordinating ligand.[24] These data revealed an energy level of the relaxed excited ILCT state [E(ILCT*)] is at about 26 500 cm^{-1}, whilst the triplet state associated with the phosphorescence of the Gd(III) complex shows an energy position at 20 830 cm^{-1}. A comparison with the energy levels of the accepting Yb(III) state (in the 10 000–11 000 cm^{-1} range) clearly indicates the presence of a big energy gap between the donor and acceptor levels, which could negatively impact the ligand-to-metal energy transfer efficiency.

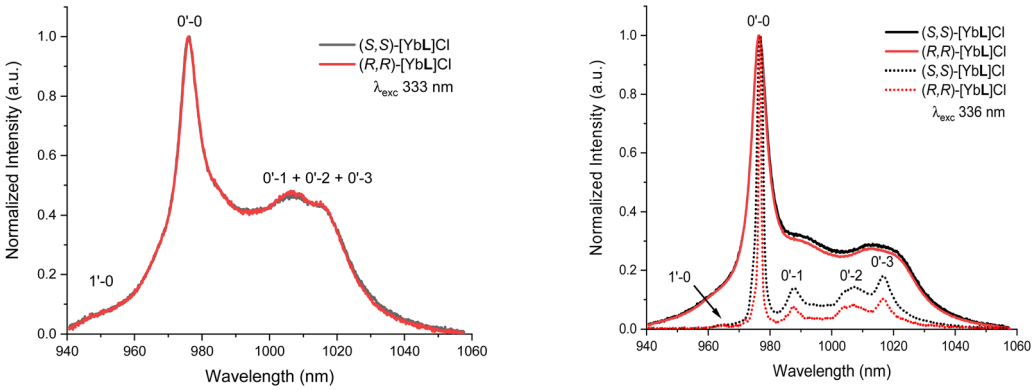

Fig. 7 (left) Room temperature normalized luminescence emission spectra of (*S*,*S*)-[Yb**L**]Cl and (*R*,*R*)-[Yb**L**]Cl in water solution (10^{-6} M). Excitation at 333 nm. (right) Overlap of normalized luminescence emission spectra of (*S*,*S*)-[Yb**L**]Cl and (*R*,*R*)-[Yb**L**]Cl in methanol/ethanol (1/4 v/v) solution (10^{-6} M) at room temperature (solid lines) and at 77 K (dotted lines). Excitation at 336 nm.

Nevertheless, the sensitization of the Yb(III) emission is not usually accounted for in the frame of the classical Förster–Dexter theory, precisely when a large mismatch between the involved electronic levels is present. So far, three mechanisms have been invoked in this context. The first one occurs by an internal redox process involving the Yb(III)/Yb(II) redox couple and the excited state of the ligand[43] while the second proceeds *via* an internal conversion inside the energy levels of the Yb(III)-ligand system considered as a single chromophore.[44] The third mechanism foresees the involvement of a ligand-to-metal charge transfer (LMCT) state.[45–47] In the present case, the available information does not allow us to discriminate among the three proposed mechanisms and the in-depth study of this aspect is beyond the scope of the present contribution.

The luminescence decay curve of the Yb(III) $^2F_{5/2}$ excited state can be fitted by a single exponential function in all the employed solvents (water, deuterated water, methanol, deuterated methanol; Fig. 8 and Fig. S6, ESI†).

For both water and methanol, the calculated $^2F_{5/2}$ lifetime increases significantly when the deuterated solvent is used (Table 1). This is in agreement with the presence of solvent molecules in the inner coordination sphere of the complexes capable of quenching the Yb(III) excited state by means of a non radiative multiphonon relaxation (MPR) process.[48] This process is favored by the presence of one (in the case of methanol) or two (in the case of water) sources of high energy (O–H) vibrations, with a concomitant decrease in the lifetime. In contrast, O–D vibrations in the close proximity of the metal ion are much less efficient in the quenching of Yb(III) luminescence and the value of the excited state lifetime is higher. It is possible to estimate q and m, that are the number of water and methanol molecules in the inner coordination sphere, by using the equations $q = \frac{1}{\tau_{H_2O}} - \frac{1}{\tau_{D_2O}} - 0.20$ and $m = 2 \cdot \left(\frac{1}{\tau_{MeOH}} - \frac{1}{\tau_{MeOD}} - 0.10\right)$, where τ is the $^2F_{5/2}$ observed lifetimes in μs.[49] We calculate the values of q = 1 and m = 0.2, indicating that no solvent molecules are bound to the metal center in the case of methanol. In contrast, one water molecule is present in the first coordination sphere, as observed in the DFT minimum energy structure reported in Fig. 3. The change of Yb(III) coordination number (9 in water, 8 in methanol) could explain the observed differences in the chiroptical properties, such as NIR-ECD spectra (Fig. 6 and Fig. S5, ESI†) and NIR-CPL spectra (Fig. 9).

The capability of the enantiopure complexes to emit circularly polarized luminescence was studied by means of a home-made setup.[34] Indeed, upon excitation at 365 nm (in the ILCT

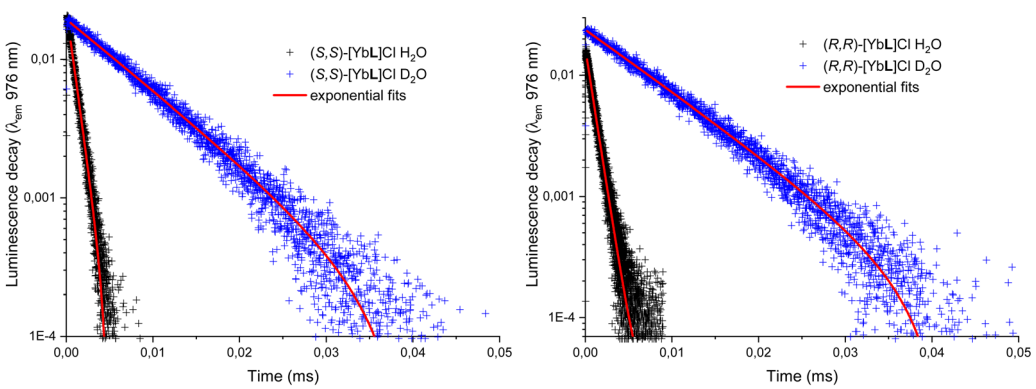

Fig. 8 Luminescence decay of the $^2F_{5/2}$ level of Yb(III) for both the enantiomers (*S*,*S*) (left) and (*R*,*R*) (right) of [Yb**L**]Cl complex in water and deuterated water. Excitation at 333 nm.

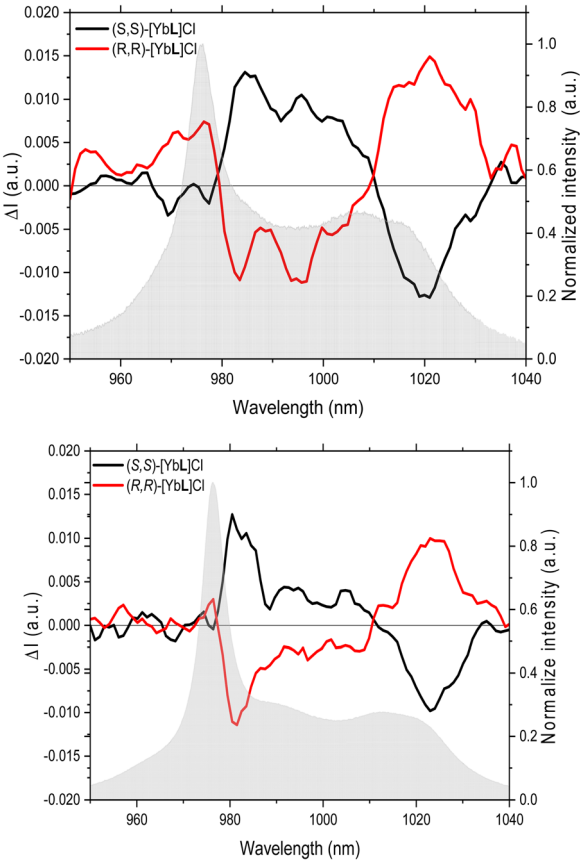

Fig. 9 CPL spectra of (*S,S*)-[Yb**L**]Cl and (*R,R*)-[Yb**L**]Cl complexes in water (up) and in methanol (bottom) emitting in the near infrared region. Excitation at 365 nm.

transition), the two enantiomers of the [Yb**L**]Cl complex show a NIR CPL mirror image, both in water and methanol (Fig. 9).

The extent of the luminescence chiroptical activity, quantified by the values of g_{lum} (in the 0.01–0.04 range; Table 1) is in line with already reported examples of Yb(III) chiral complexes.[11,50] As we recently demonstrated for the ligand **L**,[24] the same excited state involved in the sensitization process of Eu(III) and Sm(III) luminescence (and Yb(III) in the present contribution) can be efficiently populated by both 1P and 2P excitation (at 337 nm and 720 nm, respectively). Hence, the emission of the complex does not depend on the nature of the sensitization process and the corresponding excitation source (1P or 2P excitation). Transferring this approach on the respective chiroptical properties, we can reasonably assume that (even though we do not directly prove that) the same CPL signal can be triggered upon both 1P and 2P excitation. The possibility of obtaining CPL at NIR wavelengths upon excitation in the same spectral range (720 nm) paves the way for the design of a new generation of lanthanide(III) complexes as potential NIR-to-NIR chiroptical probes for biomedical applications.

Conclusions

In this contribution, new Yb(III)-based enantiomeric complexes are synthesized and characterized from a thermodynamic and a spectroscopic point of view. The obtained high stability of the Yb**L** species and selectivity with respect to Zn(II) and Ca(II) prevent the competition and release of the metal ion in the biological medium, which is an essential feature of a metal complex to be potentially employed in bioimaging experiments.

DFT calculations suggest that among the three possible isomeric complexes, differing by the stereochemistry at sp^3 N atoms of ligand **L** (*trans*-OO, *trans*-NN and *cis*-OO,NN), the latter one is dominant in aqueous solution. It is noteworthy that the Yb(III) luminescence in the NIR is circularly polarized (the highest g_{lum} value is |0.04| at 1021 nm) and can be efficiently sensitized upon excitation of the ligand into the picolinate-based absorption band at about 330 nm. As it is well known that this antenna exhibits a good two-photon cross-section (around 110 GM, at 700 nm), the Yb(III) luminescence can also be potentially triggered by excitation in the NIR spectral region. As the same electronic transition of the picolinate antenna, showing a charge transfer (CT) character, can be triggered by 2P absorption and the Ln(III) emission is not affected by the nature of the sensitization process (1P or 2P excitation), we can reasonably assume that the observed CPL signal can be obtained upon both 1P (in the UV range) and 2P (in the NIR range) excitation of the ligand. Our Yb(III)-based chiroptical complex is expected to play an important role in emerging chiroptical applications in the biological field, such as the study of live cell chiral molecular interactions. All that could be also applied in *in vivo* experiments, as [Yb**L**]Cl can completely work in the so-called biological windows.

Author contributions

OM, AM and FP: conceptualization, writing the original draft; SM, AS and MS: investigation and methodology; SR and FB: supervision and data curation; LG, BB, AB-L, YG and SG: formal analysis and validation.

Conflicts of interest

There are no conflicts to declare.

Acknowledgements

SM, SR, MS, AM and FP thank the Italian Ministry of University and Research for the received funds [PRIN (Progetti di Ricerca di Rilevante Interesse Nazionale, Bando 2022 PNRR) project "TheCURA", Grant No. P20222TPZS]. SM, SR and FP gratefully also thank the Facility "Centro Piattaforme Tecnologiche" of the University of Verona for access to the instrumentation. Funding from the University of Verona is gratefully acknowledged. Article processing charges were supported by the special fund at the University of Verona dedicated to Open Access publications. AM and MS acknowledge the University of Udine for Research financed with European Union funds – NextGenerationEU—MSCA grants D.M. 737/2021—CUPG25F21003390007. The funders had no role in study design, data collection and analysis,

decision to publish, or preparation of the manuscript. The authors thank the Agence Nationale de la Recherche (SMMCPL ANR-19-CE29-0012-02) for financial support and a grant to AS.

References

1 H.-Y. Wong, W.-S. Lo, K.-H. Yim and G.-L. Law, *Chem*, 2019, **5**, 3058–3095.
2 Y. Kitagawa, S. Wada, M. D. J. Islam, K. Saita, M. Gon, K. Fushimi, K. Tanaka, S. Maeda and Y. Hasegawa, *Commun. Chem.*, 2020, **3**, 1–5.
3 O. G. Willis, F. Zinna and L. Di Bari, *Angew. Chem., Int. Ed.*, 2023, **62**, e202302358.
4 O. G. Willis, F. Petri, G. Pescitelli, A. Pucci, E. Cavalli, A. Mandoli, F. Zinna and L. Di Bari, *Angew. Chem., Int. Ed.*, 2022, **61**, e202208326.
5 N. F. M. Mukthar, N. D. Schley and G. Ung, *J. Am. Chem. Soc.*, 2022, **144**, 6148–6153.
6 B.-A. N. Willis, D. Schnable, N. D. Schley and G. Ung, *J. Am. Chem. Soc.*, 2022, **144**, 22421–22425.
7 O. G. Willis, A. Pucci, E. Cavalli, F. Zinna and L. Di Bari, *J. Mater. Chem. C*, 2023, **11**, 5290–5296.
8 K. Dhbaibi, M. Grasser, H. Douib, V. Dorcet, O. Cador, N. Vanthuyne, F. Riobé, O. Maury, S. Guy, A. Bensalah-Ledoux, B. Baguenard, G. L. J. A. Rikken, C. Train, B. Le Guennic, M. Atzori, F. Pointillart and J. Crassous, *Angew. Chem., Int. Ed.*, 2023, **62**, e202215558.
9 B. Lefeuvre, C. A. Mattei, J. F. Gonzalez, F. Gendron, V. Dorcet, F. Riobé, C. Lalli, B. Le Guennic, O. Cador, O. Maury, S. Guy, A. Bensalah-Ledoux, B. Baguenard and F. Pointillart, *Chem. – Eur. J.*, 2021, **27**, 7362–7366.
10 J. A. Adewuyi, N. D. Schley and G. Ung, *Chem. – Eur. J.*, 2023, **29**, e202300800.
11 E. Cavalli, C. Nardon, O. G. Willis, F. Zinna, L. Di Bari, S. Mizzoni, S. Ruggieri, S. C. Gaglio, M. Perduca, C. Zaccone, A. Romeo and F. Piccinelli, *Chem. – Eur. J.*, 2022, **28**, e202200574.
12 O. G. Willis, F. Zinna, G. Pescitelli, C. Micheletti and L. Di Bari, *Dalton Trans.*, 2022, **51**, 518–523.
13 L. Wang, Z. Yao, W. Huang, T. Gao, P. Yan, Y. Zhou and H. Li, *Inorg. Chem. Front.*, 2023, **10**, 3664–3674.
14 J. Yuasa, T. Ohno, H. Tsumatori, R. Shiba, H. Kamikubo, M. Kataoka, Y. Hasegawa and T. Kawai, *Chem. Commun.*, 2013, **49**, 4604–4606.
15 S. Orsini, F. Zinna, T. Biver, L. D. Bari and I. Bonaduce, *RSC Adv.*, 2016, **6**, 96176–96181.
16 M. Leonzio, A. Melchior, G. Faura, M. Tolazzi, M. Bettinelli, F. Zinna, L. Arrico, L. Di Bari and F. Piccinelli, *New J. Chem.*, 2018, **42**, 7931–7939.
17 M. Leonzio, A. Melchior, G. Faura, M. Tolazzi, F. Zinna, L. Di Bari and F. Piccinelli, *Inorg. Chem.*, 2017, **56**, 4413–4422.
18 P. Stachelek, L. MacKenzie, D. Parker and R. Pal, *Nat. Commun.*, 2022, **13**, 553.
19 E. Cavalli, S. Ruggieri, S. Mizzoni, C. Nardon, M. Bettinelli and F. Piccinelli, *Results Chem.*, 2022, **4**, 100388.
20 F. Piccinelli, S. Mizzoni, G. Zanella, S. C. Gaglio, M. Perduca, A. Romeo, S. Ruggieri, C. Nardon and E. Cavalli, *Molecules*, 2023, **28**(5), 2251.
21 A. D'Aléo, A. Bourdolle, S. Brustlein, T. Fauquier, A. Grichine, A. Duperray, P. L. Baldeck, C. Andraud, S. Brasselet and O. Maury, *Angew. Chem., Int. Ed.*, 2012, **51**, 6622–6625.
22 M. Soulié, F. Latzko, E. Bourrier, V. Placide, S. J. Butler, R. Pal, J. W. Walton, P. L. Baldeck, B. Le Guennic, C. Andraud, J. M. Zwier, L. Lamarque, D. Parker and O. Maury, *Chem. – Eur. J.*, 2014, **20**, 8636–8646.
23 N. Hamon, A. Roux, M. Beyler, J.-C. Mulatier, C. Andraud, C. Nguyen, M. Maynadier, N. Bettache, A. Duperray, A. Grichine, S. Brasselet, M. Gary-Bobo, O. Maury and R. Tripier, *J. Am. Chem. Soc.*, 2020, **142**, 10184–10197.
24 S. Mizzoni, S. Ruggieri, A. Sickinger, F. Riobé, L. Guy, M. Roux, G. Micouin, A. Banyasz, O. Maury, B. Baguenard, A. Bensalah-Ledoux, S. Guy, A. Grichine, X.-N. Nguyen, A. Cimarelli, M. Sanadar, A. Melchior and F. Piccinelli, *J. Mater. Chem. C*, 2023, **11**, 4188–4202.
25 A. I. Vogel and J. Mendham, *Vogel's textbook of quantitative chemical analysis*, Prentice Hall, 2000.
26 F. Endrizzi, P. Di Bernardo, P. L. Zanonato, F. Tisato, M. Porchia, A. A. Isse, A. Melchior and M. Tolazzi, *Dalton Trans.*, 2017, **46**, 1455–1466.
27 A. C. Mendonça, A. F. Martins, A. Melchior, S. M. Marques, S. Chaves, S. Villette, S. Petoud, P. L. Zanonato, M. Tolazzi, C. S. Bonnet, É. Tóth, P. Di Bernardo, C. F. G. C. Geraldes and M. A. Santos, *Dalton Trans.*, 2013, **42**, 6046–6057.
28 G. Gran, *Analyst*, 1952, **77**, 661–670.
29 P. Gans, A. Sabatini and A. Vacca, *Talanta*, 1996, **43**, 1739–1753.
30 M. J. Frisch, G. W. Trucks, H. B. Schlegel, G. E. Scuseria, M. A. Robb, J. R. Cheeseman, G. Scalmani, V. Barone, G. A. Petersson, H. Nakatsuji, X. Li, M. Caricato, A. V. Marenich, J. Bloino, B. G. Janesko, R. Gomperts, B. Mennucci, H. P. Hratchian, J. V. Ortiz, A. F. Izmaylov, J. L. Sonnenberg, D. Williams-Young, F. Ding, F. Lipparini, F. Egidi, J. Goings, B. Peng, A. Petrone, T. Henderson, D. Ranasinghe, V. G. Zakrzewski, J. Gao, N. Rega, G. Zheng, W. Liang, M. Hada, M. Ehara, K. Toyota, R. Fukuda, J. Hasegawa, M. Ishida, T. Nakajima, Y. Honda, O. Kitao, H. Nakai, T. Vreven, K. Throssell, J. A. Montgomery Jr., J. E. Peralta, F. Ogliaro, M. J. Bearpark, J. J. Heyd, E. N. Brothers, K. N. Kudin, V. N. Staroverov, T. A. Keith, R. Kobayashi, J. Normand, K. Raghavachari, A. P. Rendell, J. C. Burant, S. S. Iyengar, J. Tomasi, M. Cossi, J. M. Millam, M. Klene, C. Adamo, R. Cammi, J. W. Ochterski, R. L. Martin, K. Morokuma, O. Farkas, J. B. Foresman and D. J. Fox, *Gaussian 16 Rev.A03*, Wallingford, CT.
31 J.-D. Chai and M. Head-Gordon, *Phys. Chem. Chem. Phys.*, 2008, **10**, 6615–6620.
32 M. Dolg, H. Stoll and H. Preuss, *J. Chem. Phys.*, 1989, **90**, 1730–1734.
33 J. Tomasi, B. Mennucci and R. Cammi, *Chem. Rev.*, 2005, **105**, 2999–3093.

34 B. Baguenard, A. Bensalah-Ledoux, L. Guy, F. Riobé, O. Maury and S. Guy, *Nat. Commun.*, 2023, **14**, 1065.
35 R. M. Smith and A. E. Martell, *Sci. Total Environ*, 1987, **64**, 125–147.
36 F. Lucio-Martínez, Z. Garda, B. Váradi, F. K. Kálmán, D. Esteban-Gómez, É. Tóth, G. Tircsó and C. Platas-Iglesias, *Inorg. Chem.*, 2022, **61**, 5157–5171.
37 M. de Guadalupe Jaraquemada–Peláez, X. Wang, T. J. Clough, Y. Cao, N. Choudhary, K. Emler, B. O. Patrick and C. Orvig, *Dalton Trans.*, 2017, **46**, 14647–14658.
38 J. A. Peters, K. Djanashvili, C. F. G. C. Geraldes and C. Platas-Iglesias, *Coord. Chem. Rev.*, 2020, **406**, 213146.
39 P. Di Bernardo, A. Melchior, M. Tolazzi and P. L. Zanonato, *Coord. Chem. Rev.*, 2012, **256**, 328–351.
40 M. Regueiro-Figueroa, D. Esteban-Gómez, A. de Blas, T. Rodríguez-Blas and C. Platas-Iglesias, *Chem. – Eur. J.*, 2014, **20**, 3974–3981.
41 P. K. Tse and J. E. Powell, *Inorg. Chem.*, 1985, **24**, 2727–2730.
42 M. Woods, K. M. Payne, E. J. Valente, B. E. Kucera and V. G. Young Jr., *Chem. – Eur. J.*, 2019, **25**, 9997–10005.
43 W. D. Horrocks, J. P. Bolender, W. D. Smith and R. M. Supkowski, *J. Am. Chem. Soc.*, 1997, **119**, 5972–5973.
44 C. Reinhard and H. U. Güdel, *Inorg. Chem.*, 2002, **41**, 1048–1055.
45 V. A. Ilichev, A. V. Rozhkov, R. V. Rumyantcev, G. K. Fukin, I. D. Grishin, A. V. Dmitriev, D. A. Lypenko, E. I. Maltsev, A. N. Yablonskiy, B. A. Andreev and M. N. Bochkarev, *Dalton Trans.*, 2017, **46**, 3041–3050.
46 A. Masuya-Suzuki, S. Goto, T. Kambe, R. Karashimada, Y. Kubota and N. Iki, *ChemistryOpen*, 2021, **10**, 46–55.
47 Y.-J. Liang, F. Liu, Y.-F. Chen, X.-J. Wang, K.-N. Sun and Z. Pan, *Light: Sci. Appl.*, 2016, **5**, e16124.
48 E. Kreidt, C. Kruck and M. Seitz, in *Handbook on the Physics and Chemistry of Rare Earths*, ed. J.-C. G. Bünzli and V. K. Pecharsky, Elsevier, 2018, vol. 53, pp. 35–79.
49 A. Beeby, I. M. Clarkson, R. S. Dickins, S. Faulkner, D. Parker, L. Royle, A. S. de Sousa, J. A. G. Williams and M. Woods, *J. Chem. Soc., Perkin Trans. 2*, 1999, 493–504.
50 F. Zinna, L. Arrico and L. D. Bari, *Chem. Commun.*, 2019, **55**, 6607–6609.

